Measurement report: Nocturnal subsidence behind the cold front enhances surface particulate matter in the plain regions: observation from the mobile multi-lidar system

Yiming Wang[1, 2], Haolin Wang[1, 2], Yujie Qin[1, 2], Xinqi Xu[1, 2], Guowen He[1, 2], Nanxi Liu[1, 2], Shengjie Miao[1, 2], Xiao Lu[1, 2], Haichao Wang[1, 2, *], Shaojia Fan[1, 2, *]

[1]School of Atmospheric Sciences, Sun Yat-sen University, and Southern Marine Science and Engineering Guangdong Laboratory (Zhuhai), Zhuhai, 519082, China
[2]Guangdong Provincial Observation and Research Station for Climate Environment and Air Quality Change in the Pearl River Estuary, Key Laboratory of Tropical Atmosphere-Ocean System (Sun Yat-sen University), Ministry of Education, Zhuhai, 519082, China

Correspondence to:
Haichao Wang (wanghch27@mail.sysu.edu.cn); Shaojia Fan (eesfsj@mail.sysu.edu.cn)

Abstract. A multi-lidar system, mounted in a vehicle to monitor the profiles of temperature, wind, and particle optical properties, was utilized to investigate the winter fine particulate matter ($PM_{2.5}$) pollution from a vertical perspective, in four cities in China in winter 2018. We observed the enhancement of surface nocturnal $PM_{2.5}$ in two typical plain cities (Changzhou and Wangdu), which was attributed to the subsidence of $PM_{2.5}$ transported from upstream polluted areas, with the wind turning north and downdrafts dominating. Combining with the observed surface $PM_{2.5}$, the reanalysis meteorological data, and the GEOS-Chem model simulation, we revealed the Transport-Nocturnal $PM_{2.5}$ Enhancement by Subsidence (T-NPES) events occurred frequently in the two cities, with percentages of 12.2 % and 18.0 %, respectively during Dec. 2018 - Feb. 2019. Furthermore, the GEOS-Chem model simulation further confirmed the ubiquity of winter T-NPES events on a large scale including North China Plain and the Yangtze River Delta. Process analysis revealed that the subsidence was closely correlated with the southeasterly movement of the high-pressure system and the passage of the cold front, resulting in the increase of temperature aloft, a stronger inversion layer, and further $PM_{2.5}$ accumulation in the atmospheric boundary layer. Thus, a conceptual model of the T-NPES events was proposed to highlight this surface $PM_{2.5}$ enhancement mechanism in these plain regions. However, it did not apply to the two cities in the basin region (Xi'an and Chengdu), due to the obstruction of the weather system movement by the mountains surrounding the basin.

1 Introduction

The severe fine particulate matter ($PM_{2.5}$, particles with an aerodynamic diameter smaller than 2.5 μm) pollution, caused by the rapid industrialization and urbanization in China (Guo et al., 2014; Huang et al., 2014), has essential impacts on visibility, ecosystem, regional and global climates, and human health (Yue et al., 2017; An et al., 2019; De Marco et al., 2019; Li et al., 2019b; Hao et al., 2021). To mitigate the $PM_{2.5}$ pollution, the government of China implemented the Air Pollution Prevention and Control Action Plan in 2013 by strict emission controls (Gao et al., 2020). Despite the fact that the annual average concentration of $PM_{2.5}$ has significantly decreased (Ding et al., 2019; Li et al., 2019a; Zhang et al., 2019b; Silver et al., 2020; Geng et al., 2021b), the $PM_{2.5}$ levels in the majority of Chinese cities are still above the World Health Organization target (WHO. 2021). Particularly, the issue of $PM_{2.5}$ pollution remained critical in the North China Plain (NCP) and Yangtze River Delta (YRD) in winter time (Peng et al., 2021; Qin et al., 2021).

The formation mechanisms of $PM_{2.5}$ pollution were complex especially in China (Guo et al., 2014; Xiao et al., 2021b), such as the high emission intensity (Zhang et al., 2019b), the rapid chemical formation of secondary particles owing to the gas phase and heterogeneous reactions (Wang et al., 2017; Lu et al., 2019; Chen et al., 2020), and the interactions within the atmospheric boundary layer (ABL) (Ding et al., 2013; Gao et al., 2016; Dong et al., 2017; Li et al., 2017). While the long-range transport also had significant impacts on the $PM_{2.5}$ pollution (Guo et al., 2014; Zhang et al., 2015; Huang et al., 2018). Cold fronts, as a common synoptic circulation in winter, were usually favorable for the quick removal of the locally accumulated pollutants in the NCP (Zhao et al., 2013; Gao et al., 2017), but conversely transport the pollutants to the YRD through a long distance (Kang et al., 2019; Huang et al., 2020; Kang et al., 2021). Zhou et al. (2023) indicated that the cold fronts could transport the precursors to the residual layer, where the secondary pollution was rapidly driven to be generated and then exacerbate near-surface air pollution as a result of the development of the daytime convective ABL. However, the above studies have focused on the impact of the horizontally transported pollutants on the downstream regions after the passage of the cold front. In comparison, few studies have been conducted on the variation in the vertical direction of particulate matter in the ABL during the passage of the cold front.

The vertical mixing exchange process between layer has great impact on local air quality and the subsidence motion is associated with the evolution of the inversion layer (Gramsch et al., 2014; Xu et al., 2018; He et al., 2022). Zhang et al. (2022) reported that the $PM_{2.5}$ concentration behind the cold front increased due to the subsidence motion and inversion layer. Zhao et al. (2023) suggested that the frontal downdrafts were an additional transport pathway in the nighttime to make a higher contribution to the ground nitrate. Both of their studies were based on the model simulations, the observational evidence of the subsidence behind the cold front and its impact on the nocturnal $PM_{2.5}$ enhancement events is still lacking. Shi et al. (2022) reported one subsidence case of particulate matter during the passage of the cold front over Wangdu, China in winter, which revealed that the subsidence was closely connected to the enhancement of nocturnal $PM_{2.5}$.

To investigate the mechanisms of nocturnal $PM_{2.5}$ enhancement triggered by subsidence, the three-dimensional spatial and temporal distribution is crucial. Many field observations of the vertical distribution of particulate matter have been performed employing various methods such as tethered balloons (Wang et al., 2021; Ran et al., 2022), airplanes (Wang et al., 2018; Fast et al., 2022), unmanned aerial vehicles (Song et al., 2021; Dubey et al., 2022) and the meteorological towers (Li et al., 2022; Yin et al., 2023). Lidar, as an active remote sensing device with high temporal and spatial resolution, has been extensively employed in atmospheric detection to obtain the profile of particulate matter, wind, and temperature. The ground-based and satellite-based lidar have been widely used to detect the vertical distribution of aerosol. In recent years, the mobile multi-lidar system has been gradually developed and has become a powerful tool for observing target species in a vertical perspective. Compared with the traditional ground-lidar system, the mobile multi-lidar system enables continuous mobile observations and provides information on the distribution of specific factors along its path and can be used as an effective supplement to other fixed lidars. Additionally, the mobile multi-lidar system can reach different cities by its portable setting in a short time to carry out fixed-point observations. The mobile lidar system has been used to carry out several observations in the past few years (Lv et al., 2020; He et al., 2021; Xu et al., 2022). He et al. (2021) investigated the vertical distribution characteristics of particulate matter in the Guanzhong Plain by using the mobile multi-lidar system. Xu et al. (2022) conducted an observational study on the three-dimensional structure of particulate matter distribution in the Guangdong-Hong Kong-Macao Greater Bay Area by using the mobile multi-lidar system and proposed a conceptual model to elucidate the vertical distribution of particulate matter under different wind and temperature conditions.

Here, we conducted the first nationwide field measurements in winter 2018 using the mobile multi-lidar system during winter 2018 in China, to investigate the vertical distribution characteristics of particulate matter in different cities. We focus on the observed nocturnal $PM_{2.5}$ enhancement events and seek insights into their characteristics and causes, by combining with the GEOS-Chem model simulation, the surface $PM_{2.5}$ observation, and meteorological reanalysis dataset. Finally, we examine the ubiquity of this phenomenon in plain regions in China and propose a conceptual model, providing detailed vertical insights into the enhancement of nocturnal surface $PM_{2.5}$.

2 Data and methods

2.1 Multi-lidar system

A multi-lidar system was installed on the mobile observation vehicle. The vehicle, a modified 7-seater Mercedes-Benz sport utility vehicle, was equipped with three lidar instruments mounted on steel bars at the rear for stability. The mobile observation routes were primarily on flat highways, and the speed was controlled to remain around 80 km/h to minimize the impact of frequent changes in speed and vehicle bumps on the measurement results.

The multi-lidar system (Everise Technology Ltd., Beijing) consisted of a 3D visual scanning micro pulse lidar (EV-Lidar-CAM), a twirling Raman temperature profile lidar (TRL20), a Doppler wind profile lidar (WINDVIEW10), a global positioning system (GPS). The 3D visual scanning micropulse lidar had a detection range of up to 30 km, a temporal resolution of 1 minute, and a vertical resolution of 15 m. The 3D lidar used an Nd: YAG laser to emit a 532 nm laser beam at a repetition frequency of 2500 Hz, which is scattered by aerosol particles in the atmosphere. The backscattered signal is utilized to calculate the aerosol extinction coefficient and depolarization ratio profile. The extinction coefficient increases with higher particle pollution concentrations, while the depolarization ratio can distinguish between spherical and non-spherical particles based on their size and shape. The Doppler wind profile lidar provides a temporal resolution of 1 minute and a vertical resolution of 50 m. It emits a rotating 1545 nm laser beam using a 10 kHz repetition rate fiber-pulse laser and measures the Doppler shift produced by the laser's backscattered signal as it passes through airborne particles such as dust, water droplets in clouds and fog, polluted aerosols, salt crystals, and biomass-burning aerosols to derive the horizontal and vertical wind speeds at any height. The Raman temperature profile lidar, based on Raman scattering theory, calculates atmospheric temperature by detecting the rotational Raman scattering signal of nitrogen or oxygen molecules in the atmosphere. Operating at a 532 nm wavelength with an Nd: YAG laser at a repetition frequency of 20 Hz, it has a temporal resolution of 5 minutes and a vertical resolution of 60 m. The quality of the data obtained by the lidar system was checked by the Integrated Environmental Meteorological Observation Vehicle before deployment. The results showed a percentage difference of less than 15% between the lidar system data and the data provided by the Shenzhen Meteorological

Tower, demonstrating the high accuracy of the lidar instrument (Xu et al., 2022). Data during the instrument malfunction, below the blind zone, and in rainy weather had been excluded. Previous studies have utilized this lidar system and demonstrated its reliability (Xu et al., 2018; He et al., 2021). The mobile observation vehicle and multi-lidar system are shown in Figure 1(a). The more details of the multi-lidar system are shown in the Table 1.

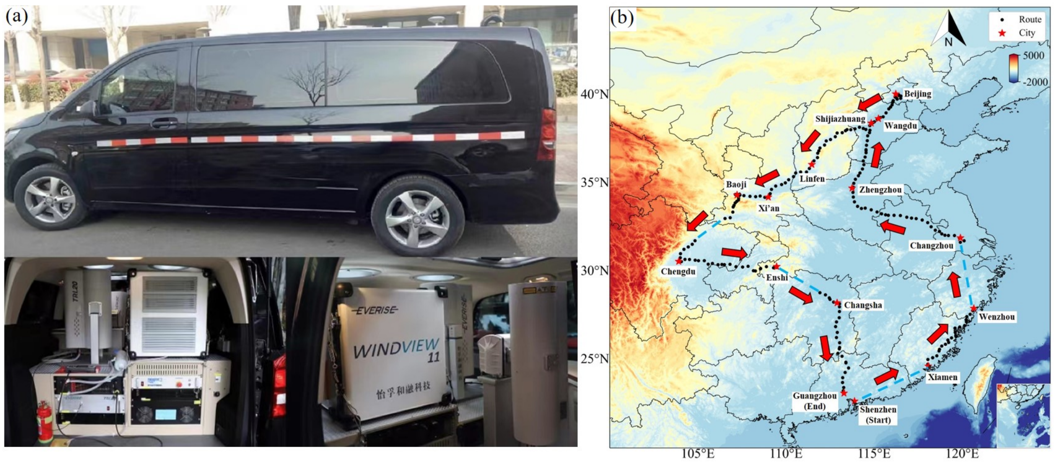

Figure 1. (a) The mobile observation vehicle and multi-lidar system. (b) For the mobile observation route and stopover cities, the blue dotted line shows the sections of missing data.

Table 1. Detailed parameters for the multi-lidar system

Lidar	Variable	Wavelength	Spatial and time resolution	Lowest observable altitude
3D visual scanning micro pulse lidar	Extinction coefficient, depolarization ratio	532 nm	15 m/1 min	30 m
Doppler wind profile lidar	Wind speed and direction profiles	1545 nm	50 m/1 min	40 m
Raman temperature profile lidar	Temperature profiles	532 nm	60 m/5 min	60 m

2.2 The route of nationwide mobile observation

To investigate the distribution characteristics of particulate matter during winter in different regions in China, the Integrated Environmental Meteorological Observation Vehicle of Sun Yat-sen University was utilized to conduct the first nationwide mobile observation campaign. The campaign, which lasted 43 days and covered approximately 11,000 km, started in Shenzhen on 30 November, 2018 and ended in Guangzhou on 11 January, 2019. This campaign surveyed the $PM_{2.5}$ vertical profiles across 15 cities, including Shenzhen, Xiamen, Wenzhou, Changzhou, Zhengzhou, Wangdu, Beijing, Shijiazhuang, Linfen, Xi'an, Baoji, Chengdu, Enshi, Changsha and Guangzhou. The observation route and stopover cities are shown in Figure 1(b). Due to the precipitation, there were no observations between Shenzhen-Xiamen and Wenzhou-Changzhou, while some GPS data were missing between Beijing-Chengdu and Enshi-Changsha.

To compare the vertical distribution characteristics of particulate matter in different regions, we conducted fixed-point observations for several pollution days in four representative cities in the East China region (Changzhou), North China Plain (Wangdu), Guanzhong Basin (Xi'an), and Sichuan Basin (Chengdu). The dates and duration of the fixed-point observations are presented in Table 2. In the following analysis, only the data obtained in the four fixed-point measurements are used since it has enough time duration to show the vertical variation of $PM_{2.5}$.

Table 2. Date and cities of fixed-point observations

Date	Cities	Coordinate	Landform
2018.12.11-2018.12.14	Changzhou	119.97°E, 31.83°N	Plain area
2018.12.18-2018.12.22	Wangdu	115.25°E, 38.67°N	Plain area
2018.12.31-2019.01.02	Xi'an	109.01°E, 34.22°N	Basin area
2019.01.04-2019.01.09	Chengdu	103.92°E, 30.58°N	Basin area

2.3 Surface $PM_{2.5}$ data and ERA5 reanalysis data

The nationwide hourly observations of surface $PM_{2.5}$ in China are obtained from the China National Environmental Monitoring Center (CNEMC) network (https://quotsoft.net/air, last accessed: March 2nd, 2023). Here, we used the hourly $PM_{2.5}$ concentration data from the whole winter of 2018 (Dec. 2018 –

Feb. 2019) and selected data from the closest monitoring station to show the change in surface $PM_{2.5}$ concentration at the four observation sites.

The spatial distribution of daily average surface $PM_{2.5}$ concentration is obtained from the TAP team (http://tapdata.org.cn), with a spatial resolution of 10 km. Based on machine learning algorithms and multi-source data information, the TAP team has built a multi-source data fusion system that integrates ground observation data, satellite remote sensing information, high-resolution emission inventories, air quality model simulations, and other multi-source information (Geng et al., 2021a; Xiao et al., 2021a). In addition to the observation data, we also apply the three-dimensional meteorological data from the ERA5 dataset for the winter of 2018 (https://quotsoft.net/air, last accessed: March 2nd, 2023) (Munoz-Sabater et al., 2021). This dataset contained temperature, horizontal and vertical wind speed, and direction at pressure levels, as well as two-dimensional data including sea-level pressure and 2-m temperature. The ERA5 dataset is the fifth generation of the European Centre for Medium-Range Weather Forecasts (ECMWF) atmospheric reanalysis of the global climate. The ERA5 dataset has a horizontal resolution of 0.25°×0.25°, a vertical resolution of 25 hPa, and a temporal resolution of 1 h.

2.4 HYSPLIT backward trajectory model

The Hybrid Single Particle Lagrangian Integrated Trajectory Model (HYSPLIT) (Stein et al., 2015), developed by NOAA Air Resources Laboratory, is a valuable tool for simulating the movement of air mass and the transport of pollutants in the atmosphere, is used in our study to obtain the sources of particulate matter at different heights. Altitudes of 100, 500, and 1000 m were set as the endpoints of the trajectories, the meteorological input for the trajectory model was the FNL dataset, and each trajectory was calculated for 24 h duration.

2.5 GEOS-Chem model description

Given the short-term (less than one week) fixed-point observation duration of the mobile observation vehicle in each city, we employ the global three-dimensional chemical transport model GEOS-Chem version 13.3.1 to interpret the vertical observations (available at https://github.com/geoschem/GCClassic/tree/13.3.1, last assessed: March 2nd, 2023, (Bey et al., 2001)) and to simulate the distribution of particulate matter concentrations during winter 2018 in China. We perform the nested-grid version of the GEOS-Chem simulation at a spatial of 0.5° (latitude) × 0.625° (longitude) resolution over East Asia (60-150°E, 11°S-55°N), The model has 47 vertical layers with 18 layers in the below 3 km. Boundary chemical conditions for the nested models are archived from a consistent global simulation run at 4° latitude × 5° longitude resolution. Meteorological input is from the Modern-Era Retrospective analysis for Research and Application version 2 (MERRA-2) (Gelaro et al., 2017). We conduct the model simulation from 2018/11-2019/02 with the first month as a spin-up.

The model mechanisms and emissions mostly follow our previous study (Wang et al., 2022). In short, the GEOS-Chem model describes a comprehensive stratospheric and tropospheric ozone–NO_x–VOCs–aerosol–halogen chemical mechanism (Wang et al., 1998; Park et al., 2004; Parrella et al., 2012; Mao et al., 2013). Photolysis rates are computed using the Fast-JX scheme (Bian and Prather. 2002). Advection of tracers in GEOS-Chem is accomplished through the TPCORE advection algorithm. The boundary layer mixing process is described in (Lin and McElroy. 2010). Dry and wet deposition of both gas and aerosols is considered (Wesely. 1989; Zhang et al., 2001). We apply the latest version of the Community Emissions Data System (CEDSv2) anthropogenic emissions inventory (O'Rourke et al., 2021) , in which the emissions over China have been adjusted to align with the Multi-resolution Emission Inventory for China (MEIC) inventory (Zheng et al., 2018). Figure S1 showed the comparison of model results with observations for monthly mean $PM_{2.5}$, and the correlation coefficients between model and observation were about 0.6, which meant that the model results provided a relatively good reproduction of the observations.

3 Results and discussions

3.1 The observation of nocturnal $PM_{2.5}$ enhancement in plain areas

During the fixed-point observation in Changzhou, we observed a typical surface $PM_{2.5}$ concentration enhancement event starting at 4:00 and lasting until 10:00 on 13 December. As shown in Figure 2(a), the concentration of $PM_{2.5}$ increased from 69 to 151 μg/m^3. Figure 2(b-c) shows the spatiotemporal distribution of the extinction coefficient and depolarization ratio. There was a clear layer with a low extinction coefficient below 500 m from 16:00 on 12 December to 4:00 on 13 December, indicating low $PM_{2.5}$ concentration near the surface. Meanwhile, an aerosol layer with a high extinction coefficient of about 0.7 km^{-1} appeared at 500-1,000 m. Figure 2(d-e) depicted the west winds prevailing in the layer of 500-1,000 m with a wind speed (WS) of about 7 m/s. Based on the daily average concentration of $PM_{2.5}$ on 12 December shown in Figure S2, the western area of the observation site in Changzhou suffered from severe air pollution with the concentration of $PM_{2.5}$ exceeding 150 μg/m^3. Under the strong forcing of the west winds, the regional transport of aerosol from the west of Changzhou was detected, leading to a high extinction coefficient layer at 500-1,000 m. The spatiotemporal distribution of the vertical velocity in Figure 2(e) indicated the dominant updraft winds in the ABL, which was conducive to the suspension of pollutants at 500-1,000 m.

However, the prevailing winds at 500-1,000 m shifted to the northwest/north after 4:00 on 13 December. By 8:00, the north wind dominated in the ABL. The change in wind direction affected the transport process of pollutants at 500-1,000 m, after which the transport basically disappeared. Meanwhile, the downdraft winds dominated above 500 m (Figure 2(e)) and the aerosol layer suspended at 500-1,000 m began to gradually transport and diffuse downward into the lower layer of ABL, which enhanced the nocturnal surface $PM_{2.5}$ concentration. Noteworthy, after 4:00 on 13 December, the surface temperature was close to the temperature at 950 hPa, suggesting that the structure of the ABL was stable and was conducive to the accumulation of the $PM_{2.5}$.

The sea surface field showed the cold high-pressure system moved southeast with increasing strength from 20:00, 12 December to 8:00, 13 December (Figure S3). The change in the synoptic weather system was accompanied by a cold frontal passage. The cold frontal passage was inferred to start at about 4:00, 13 December and last about 4 hours, which was further illustrated by the clockwise rotation of the horizontal wind from the ground to the upper layer (Shi et al., 2022) and the transition from updrafts to downdrafts, the observation site was located behind the cold front after 4:00 where the descending movements dominated. Under the influence of the subsidence, the pollutants transported by the west advection diffused downward to the low layer and further aggravated the local air quality.

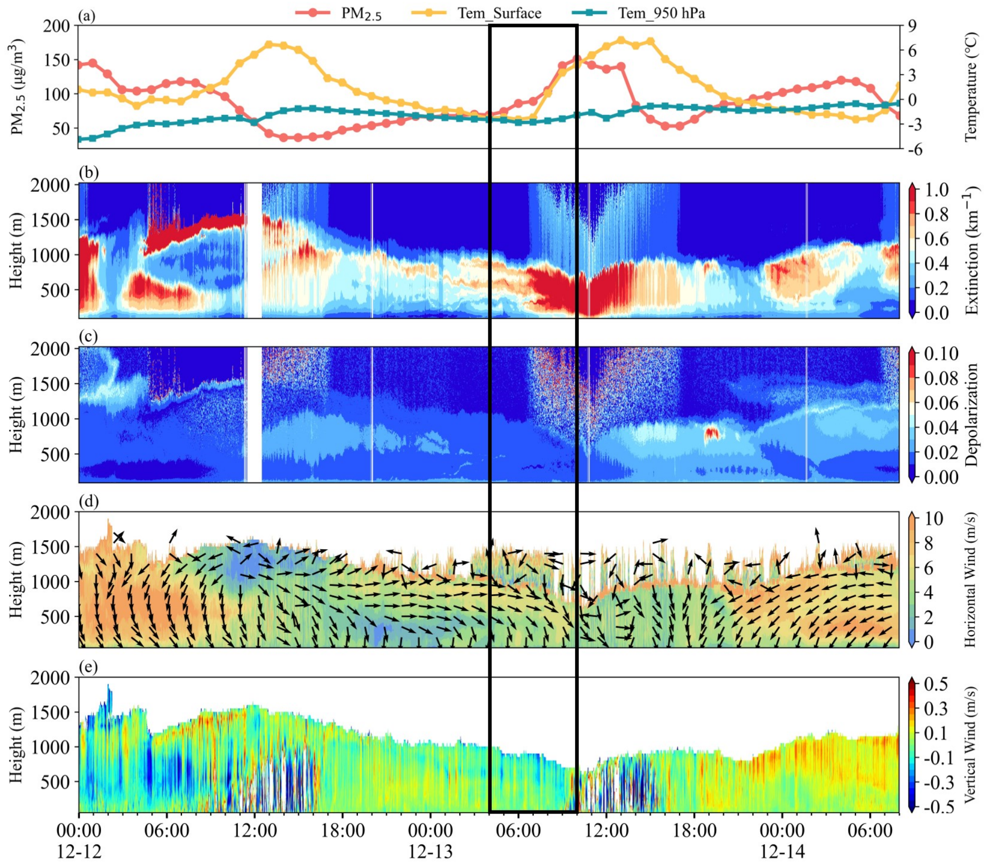

Figure 2. (a) Surface $PM_{2.5}$ concentration, surface temperature, and 950 hPa temperature, (b) Extinction coefficient, (c) Depolarization ratio, (d) Horizontal wind, and (e) Vertical wind, during the observation in Changzhou from 12 December to 14 December. The black box indicated the nocturnal surface $PM_{2.5}$ enhanced event.

After 8:00, the concentration of surface $PM_{2.5}$ increased rapidly and peaked at around 10:00, the extinction coefficient below 1,000 m also reached a high level with 1.0 km^{-1} at the same time and the depolarization remained at about 0.01. The surface temperature began to rise and the convective ABL developed rapidly, which enhanced the vertical mixing and resulted in the rapid increase in surface $PM_{2.5}$ (Zhou et al., 2023). And the north winds following the passage of the cold front dominated in the ABL after 8:00, which could bring pollution from the NCP to the YRD (Kang et al., 2019; Huang et al., 2020). Therefore, we attribute the increase in the concentration of surface $PM_{2.5}$ from 4:00 to 10:00 to the combination of the subsidence behind the cold front before 8:00, vertical mixing caused by the development of the convective ABL, and the transport by the north winds.

We also found similar nocturnal surface $PM_{2.5}$ enhancement events during the fixed-point observation in Wangdu, on 19 December and 21 December respectively (Figure 3(a)). The concentration of $PM_{2.5}$ started to enhance at 1:00, 19 December, and meanwhile, the layer of pollutants above 1,000 m started to transport and diffuse to the lower layer of ABL which was reflected by the change of the extinction coefficient shown in Figure 3(b). Unfortunately, due to the instrument malfunction, the wind profile data was unavailable and we used the ERA5 data instead, which previously showed good consistency with the observation of with Doppler wind lidar (Shi et al., 2022). As shown in Figure 3(d), from 10:00, 18 December to 0:00, 19 December, southwest winds prevailed above 1,000 m and the WS exceeded 8 m/s, a persistent southerly wind could result in severe air pollution in the NCP (Cai et al., 2017; Callahan et al., 2019; Zhang et al., 2019a). The wind forced the regional advection of pollutants from the south region suffering from serious air pollution (Figure S4) to the observation site. Meanwhile, the updrafts dominated in the ABL which facilitated the suspension of pollutants in the upper layer. After 0:00, 19 December, as the cold high-pressure system moved southwest accompanied by a cold front (Figure S5), the prevailing winds above 1,000 m shifted to the northwest gradually and downdrafts dominated behind the cold frontal passage. The changes in the horizontal and vertical wind fields caused the advection of pollutants to disappear basically and the pollutants layer suspended above 1,000 m began to transport and diffuse downward to the low layer of ABL. The passage of the cold front at 0:00, 19 December, lasted for 4 hours, and the subsidence behind the cold front caused the pollutants to diffuse downward, enhancing the concentration of nocturnal $PM_{2.5}$.

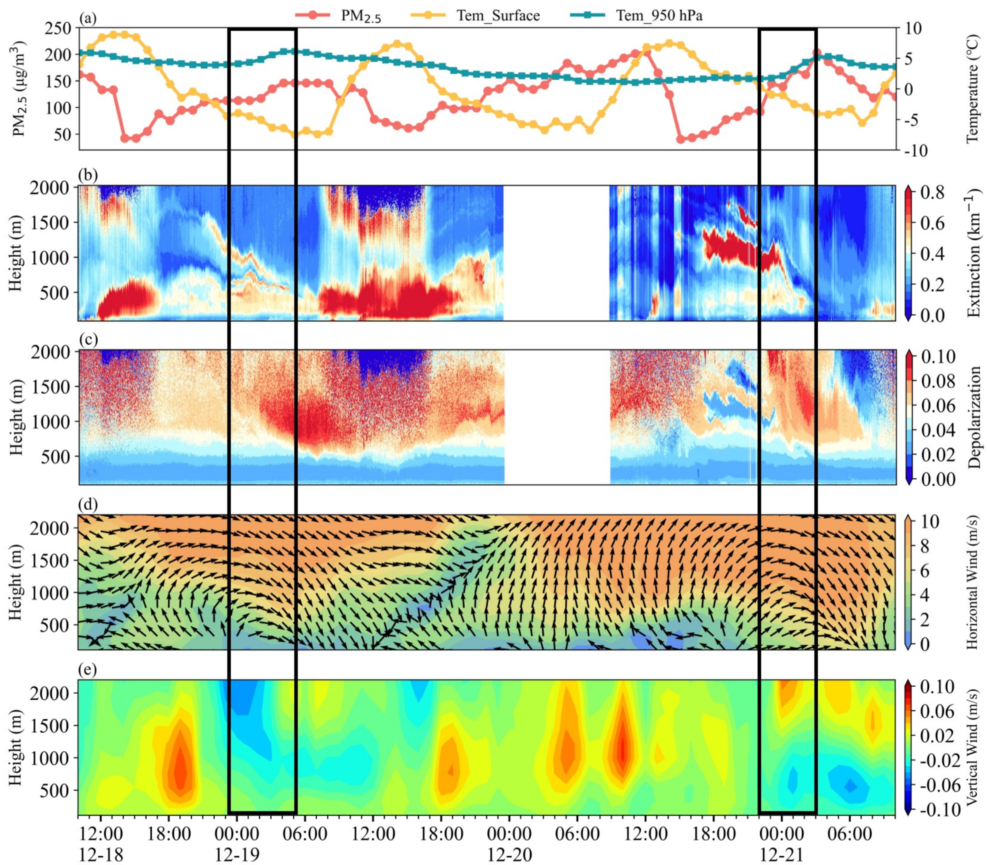

Figure 3. (a) Surface PM2.5 concentration, surface temperature, and 950 hPa temperature, (b) Extinction coefficient, (c) Depolarization ratio, (d) Horizontal wind, and (e) Vertical wind, during the observation in Wangdu from 18 December to 21 December. The black boxes indicated the Nocturnal PM2.5 enhancement events.

The pattern of the nocturnal surface PM2.5 enhancement event on 21 December was highly similar to that on 19 December. However, the pollutant advection process lasted a longer duration which started at 16:00, 20 December and ended at 0:00, 21 December (Figure 3(b)), and the WS of the southwest wind above 1,000 m exceeded 12 m/s meeting the standard of the low-level jet (LLJ) (Kraus et al., 1985; Hu et al., 2013). The area south of the observation site in Wangdu suffered from more severe air pollution with the concentration of PM2.5 exceeding 300 μg/m^3 (Figure S6). Under the strong forcing of the southwestern LLJ and the updrafts depicted in Figure 3(d-e), an aerosol layer with high extinction coefficient exceeding 2 km^{-1} formed and was suspended at 1,000-1,500 m from 16:00, 20 December to

0:00, 21 December. Meanwhile, Figure 3(c) showed that the layer with low depolarization was consistent with the layer with a high extinction coefficient, further confirming the role of transportation.

After 0:00, the wind direction of LLJ began to change due to the southeasterly movement of the high-pressure system accompanied by a cold front (Figure S7). The passage of the cold front started at 0:00, 21 December, and lasted for 4 hours, after which the downdrafts dominated below 1,500 m (Figure 3(e)), and the northwestern LLJ no longer transported pollutants from the southern area but greatly enhanced the turbulent mixing (Shi et al., 2022). Under the influence of the turbulence generated by LLJ and subsidence behind the cold front, the aerosol-rich layer suspended at 1,000-1,500 m was gradually transported and diffused downward into the lower layer of ABL, ultimately enhancing the concentration of surface $PM_{2.5}$, which was consistent with the result reported by Shi et al. (2022), with the secondary inorganic aerosol increasing simultaneously during the subsidence process as observed by the tethered balloon.

Noteworthy, when both nocturnal surface $PM_{2.5}$ enhancement events in Wangdu occurred, the temperature at 950 hPa showed an increasing trend as a result of the heating of the air by compression as it descended, while the surface temperature continuously declined (Figure 3(a)). The opposite variation of surface temperature and temperature at 950 hPa stabilized the lower atmosphere. The stronger inversion layer was probably induced by subsidence (Carlson and Stull. 1986). With the more stable atmospheric layer and inversion during subsidence, the concentration of surface $PM_{2.5}$ enhanced (Gramsch et al., 2014; Largeron and Staquet. 2016).

3.2 Transport-Nocturnal $PM_{2.5}$ Enhancement by Subsidence Events

During the fixed-point observation, we found the causes of three nocturnal $PM_{2.5}$ enhancement events in different cities were similar. The processes can be summarized as three steps: First, the horizontal winds with high wind speed forced the transport of pollutants from the upstream region, while the updrafts dominated, resulting in the formation and suspension of an aerosol layer with high extinction coefficient at the high layer of the ABL. Then, under the influence of the southeasterly movement of the high-pressure system and the passage of the cold front, the horizontal wind direction shifted to the north or northwest and the downdrafts became dominant. Finally, the transport of pollutants disappeared due to the change of wind direction, and under the subsidence behind the cold front, the aerosol-rich layer suspended at the high layer was gradually transported and diffused downward into the lower layer of the

ABL, ultimately enhancing the concentration of nocturnal $PM_{2.5}$. Here, we defined this pollution pattern as T-NPES (Transport-Nocturnal $PM_{2.5}$ Enhancement by Subsidence) events.

To investigate the occurrence frequency of T-NPES events, we employed the GEOS-Chem model to simulate the distribution of particulate matter concentrations in China during the whole winter of 2018 (Dec. 2018 – Feb. 2019). We utilized the simulated $PM_{2.5}$ at 950 hPa and 900 hPa to represent the high-altitude $PM_{2.5}$ concentration. We selected the closest grid data of the wind field data, 950 hPa, and 2-m temperature data from the ERA5 dataset to the observation site in Changzhou and Wangdu to show the meteorological condition. By analyzing the hourly concentration variation of $PM_{2.5}$ and the distribution of the wind field during the three months of winter 2018 in Changzhou and Wangdu, we found 11 typical T-NPES events in Changzhou accounting for 12.2% and 18 T-NPES events in Wangdu accounting for 18%, which indicated that the T-NPES events were a relatively common phenomenon in the two cities.

Figure 4 shows the average pattern of all T-NPES events in Changzhou, the trend of the simulated $PM_{2.5}$ was consistent with the observation, confirming the credibility of the simulations. As shown in Figure 4(a), the enhancement of nocturnal surface $PM_{2.5}$ started at 21:00, when there was no significant enhancement in anthropogenic $PM_{2.5}$ emissions, while the high-altitude $PM_{2.5}$ represented by $PM_{2.5}$ at 900 hPa and 950 hPa started to decrease, which was consistent with the observed event in Changzhou described in Section 3.1. According to the distribution of the wind field (Figure 4(b)), west winds with high wind speed prevailed in the layer above 1,000 m from 0:00 to about 18:00, which was conducive to the transport of pollutants. The updrafts dominated from 0:00 to 12:00, forcing the pollutants suspending in the upper layer, which was reflected by the enhancing $PM_{2.5}$ concentration at high altitude (Figure 4(a)). Despite the downdrafts dominating after 12:00, there was no immediate reduction in $PM_{2.5}$ concentration at high altitudes, which might be related to the fact that the horizontal wind direction had not changed, and the transport of pollutants continued. A brief updraft before 21:00 suspended the pollutants at high altitudes. After 21:00, northwester winds and downdrafts dominated in the ABL and the high-altitude $PM_{2.5}$ began to gradually transport and diffuse downward causing the enhancement of surface concentration of $PM_{2.5}$, and this process continued until 4:00 in the next day. The surface temperature and the temperature at 950 hPa gradually approached, which is consistent with the observed case in Changzhou, indicating that the structure of the ABL was stable and was conducive to the accumulation of the $PM_{2.5}$. As shown in Figure S8, the average sea level pressure indicated that the southeasterly movement of the high-pressure system and the passage of the cold front, which resulted in the shift in wind direction and subsidence behind the cold front, were the main causes of the T-NPES events.

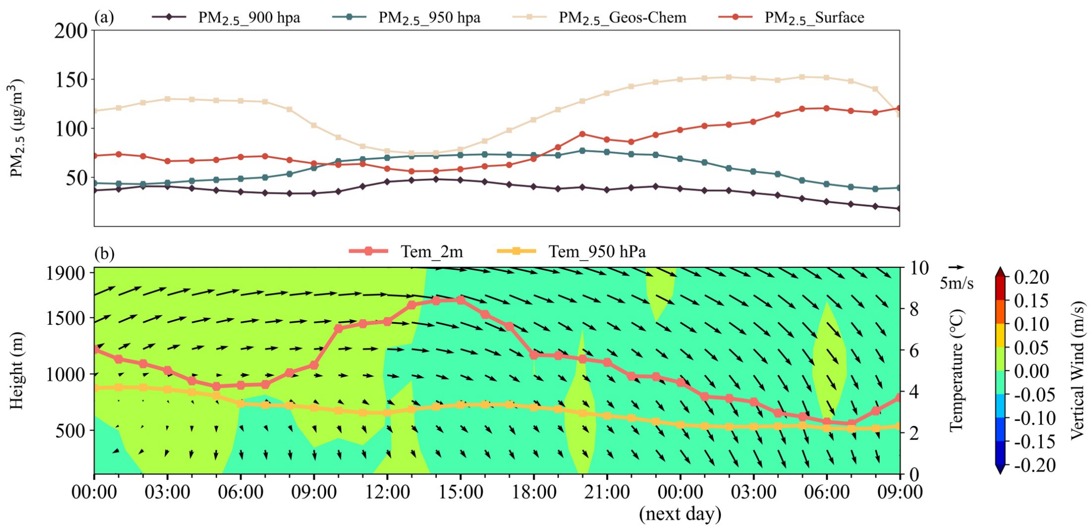

Figure 4. The average for all T-NPES events in Changzhou. (a) The concentration of $PM_{2.5}$ at different levels, surface $PM_{2.5}$ of observation (red line), surface $PM_{2.5}$ of simulation (blue line), and $PM_{2.5}$ at 900 hPa and 950 hPa. (b) The horizontal winds (arrows), the vertical winds (shaded), the temperature at 2 m, and temperature at 950 hPa.

Figure 5 shows the average pattern of all T-NPES events in Wangdu, which was similar to that in Changzhou. Figure 5(a) demonstrated that the trend of simulated $PM_{2.5}$ was consistent with the observation before 22:00 but was different thereafter. The trend of high-altitude $PM_{2.5}$ was increasing before 15:00 due to the transport of pollutants by prevailing southwester horizontal winds and the dominance of updrafts which suspended the aerosol shown in Figure 5(b). After 18:00, the prevailing winds began to turn northwest and ultimately turn north at 0:00 in the next day, while a brief updraft between 18:00 and 20:00 suspended the pollutants at high altitude. The ABL was dominated by the northwestern winds and downdrafts after 21:00. Simultaneously, the high-altitude $PM_{2.5}$ began to gradually transport and diffuse downward causing the enhancement of surface concentration of $PM_{2.5}$. The temperature at 950 hPa increased and the surface temperature declined (Figure 5(b)), which agreed with the two observation examples in Wangdu. The opposite variation of temperature at different heights stabilized the ABL and further enhanced the concentration of $PM_{2.5}$. By analyzing the weather circulation patterns, the causes of the T-NPES events were the same as those in Changzhou and were attributed to the southeasterly movement of the high-pressure system and the passage of the cold front (Figure S9).

Overall, the average patterns of T-NPES events in Changzhou and Wangdu were essentially in good agreement with the three cases of T-NPES in the two cities. But there were still slight differences, such as the change of Wangdu caused by the movement of high-pressure lasted a longer time in the average situation and the start time of subsidence behind the cold front was also not consistent, which were due to each T-NPES event was not exactly the same.

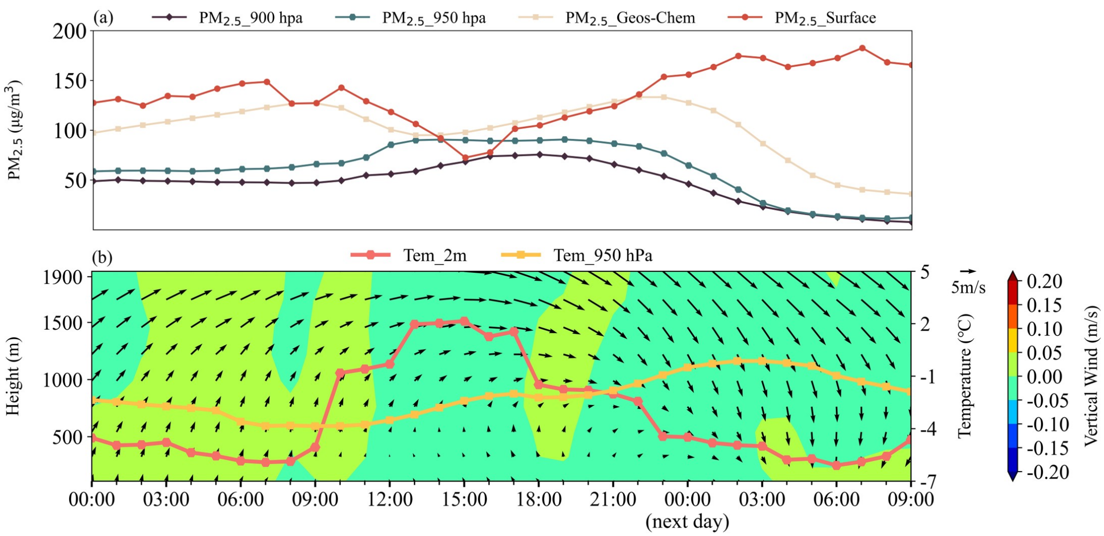

Figure 5. The average for all T-NPES events in Wangdu. (a) The concentration of $PM_{2.5}$ at different levels, surface $PM_{2.5}$ of observation (red line), surface $PM_{2.5}$ of simulation (blue line), and $PM_{2.5}$ at 900 hPa and 950 hPa. (b) The horizontal winds (arrows), the vertical winds (shaded), the temperature at 2 m, and temperature at 950 hPa

3.3 The universality of T-NPES events in eastern China

Despite the mobile observation vehicle had no observations in other cities of the NCP, the YRD, and the Loess Plateau, we could still utilize the simulated data and the ERA5 data to investigate the universality of T-NPES events occurrence in other cities. We selected Shijiazhuang, Beijing, and Tianjin as represented cities of the NCP, Shanghai, and Nanjing as represented cities of the YRD, and Taiyuan, Linfen as represented cities of the Loess Plateau. We found a similar pattern of T-NPES events in all these cities. However, these T-NPES events in different cities had some differences in detail. Here we divided the T-NPES events into four types based on the status of $PM_{2.5}$ after T-NPES events. More information on the types, frequency of the T-NPES events, and their percentage of the winter 2018 was shown in Table 3. The typical representation of Type 1 is shown in Figure 6, the characteristic of Type 1 was that the southwestern winds transported the pollutants in the high-altitude of the ABL, then the wind direction shifted to north and downdrafts dominated, finally, pollutants in high-altitude diffused into lower layer causing the surface $PM_{2.5}$ enhanced. However, after the T-NPES event, the north wind near the ground was not strong enough to remove the pollutants, causing a high level of $PM_{2.5}$ lasting the next day morning and may result in aggravation of the air pollution in the following day. The characteristic of the T-NPES event of Type 2 was basically consistent with Type 1. However, after the T-NPES event, as north winds became stronger, pollutants were rapidly removed, resulting in a clean boundary layer throughout (Figure 7). Even when the pollutants were removed more quickly by stronger north winds, the subsidence process might not be observed. Type 1 and Type 2 were both observed in the NCP cities, while Type 1 predominated in Wangdu and Shijiazhuang, and Type 2 in Beijing and Tianjin.

Table 3. Statistics of the T-NPES events in cities during Dec. 2018 – Feb. 2019

Area	Type	City	Frequency (days)	Percentages
NCP	Type 1 and 2	Wangdu	18	20.0%
		Shijiazhuang	18	20.0%
		Beijing	13	14.4%
		Tianjin	14	15.6%
YRD	Type 3	Changzhou	11	12.2%
		Shanghai	7	7.8%
		Nanjing	8	8.9%
Loess Plateau	Type 4	Linfen	18	20.0%
		Taiyuan	13	14.4%

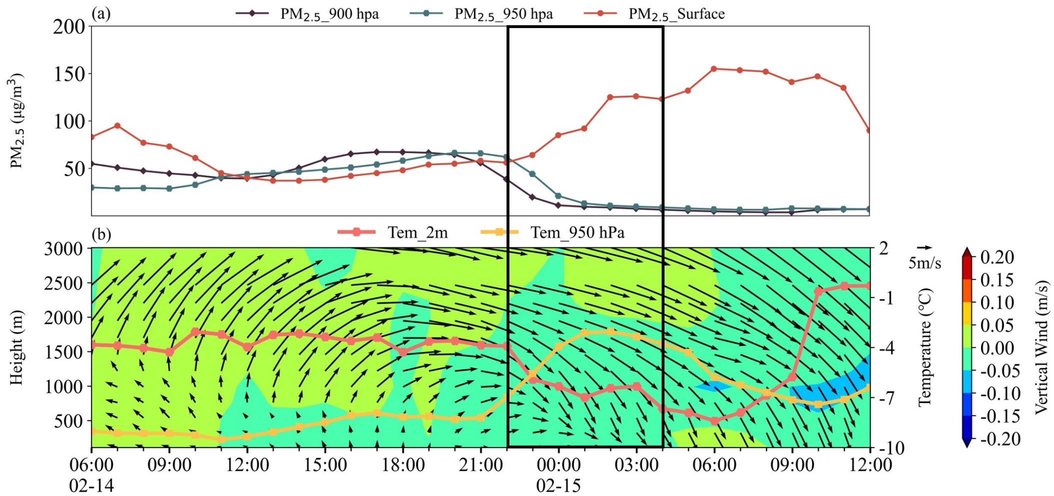

Figure 6. A typical T-NPES event of Type 1. The black box indicated the T-NPES event.

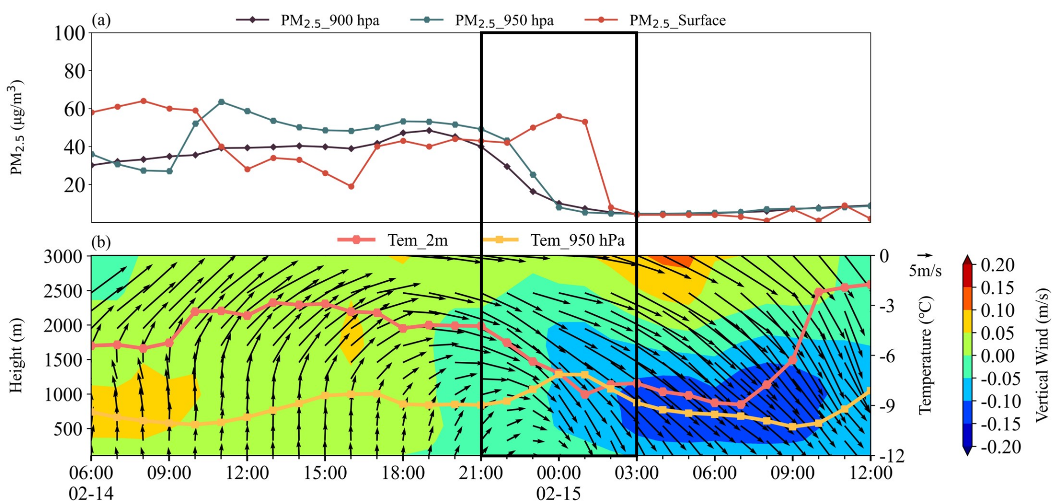

Figure 7. A typical T-NPES event of Type 2. The black box indicated the T-NPES event.

Figure 8 shows the typical representation of Type 3. The prevailing wind transporting pollutants was not southwest but west and the start and end of the T-NPES event were later than for Type 1 and 2. After the T-NPES event, the increase of 2-m temperature and the development of convective ABL led to vertical mixing and the increase of surface $PM_{2.5}$. Additionally, the stronger north wind might transport the pollutants from the NCP to the YRD. Type 3 was similar to the example in Changzhou in Section 3.1 and indicative of a typical pattern in the YRD cities.

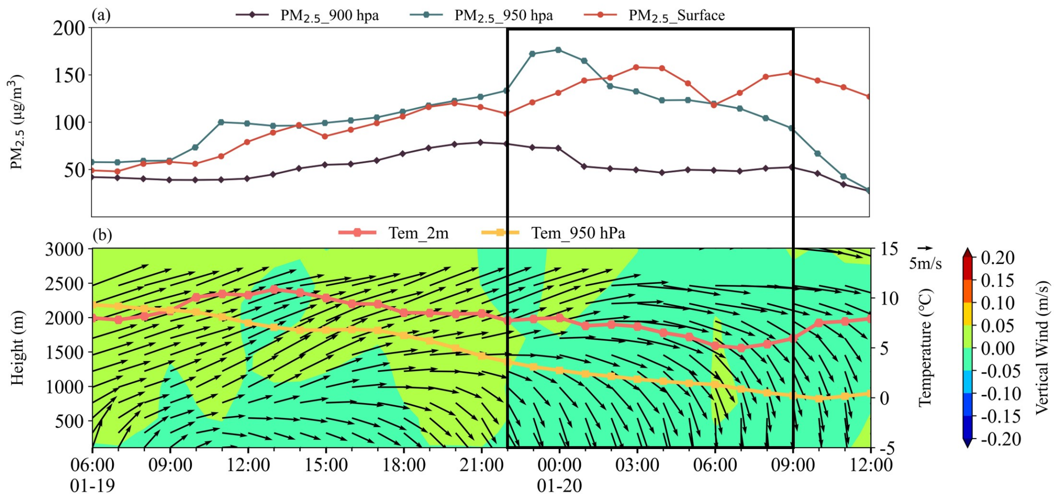

Figure 8. A typical T-NPES event of Type 3. The black box indicated the T-NPES event.

The typical representation of Type 4, which mainly occurred in the Loess Plateau cities, was shown in Figure 9. During the T-NPES event, the change of wind direction was only observed above 1,500 m while the wind speed below was so weak that the shift in wind direction was not significant, which was significantly different from the wind field of the other three types. The reason for the difference between Type 4 and other types was mainly related to the topography of the Loess Plateau, which has a blocking effect on the movement of the high-pressure system. Noteworthy, after the analysis of these T-NPES events in different cities in China, we suggested that the T-NPES events were a common pattern of the nocturnal $PM_{2.5}$ enhancement, but did not always have an impact on the air pollution of the following day. The pollution levels on the following day depended more on the strength of the cold front, local pollution conditions, the structure of ABL, and regional transportation. Further quantification is needed to determine the relationship between the T-NPES events and the pollution levels on the following day.

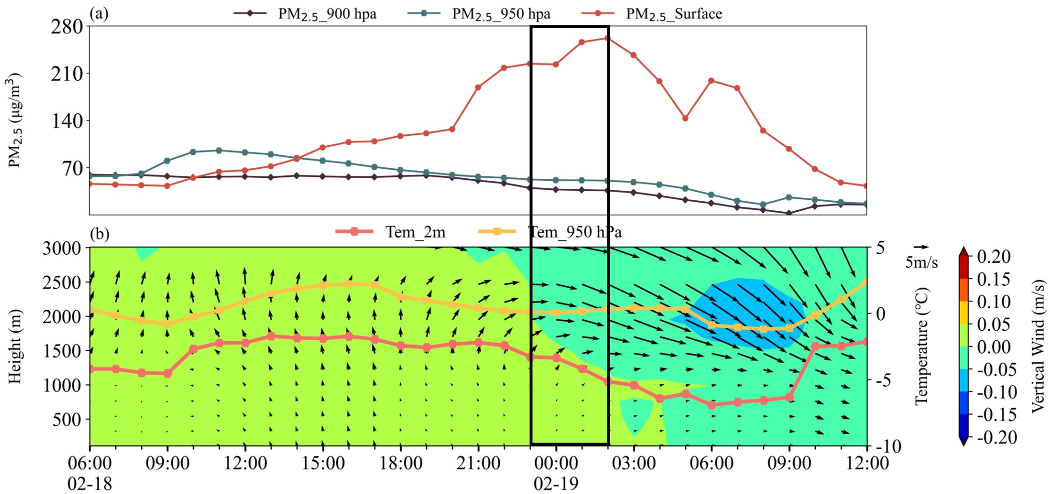

Figure 9. A typical T-NPES event of Type 4. The black box indicated the T-NPES event.

To look insights into the mechanism of nocturnal $PM_{2.5}$ enhancement, we systematically documented instances of nocturnal $PM_{2.5}$ enhancement during the winter of 2018 in Wangdu and Changzhou according to the surface $PM_{2.5}$ observation. We identified 48 such events in Wangdu and 27 in Changzhou, with proportions of T-NPES events of 37.5% and 40.7%, respectively. The results implied that T-NPES represents merely one among multiple pathways contributing to the nocturnal $PM_{2.5}$ enhancement. We checked the nocturnal $PM_{2.5}$ enhancement events that were not caused by T-NPES in Wangdu, the dominant wind field distributions within the ABL were southerly or characterized by static light wind, which indicated that the nocturnal $PM_{2.5}$ enhancement might result from either horizontal transport from polluted regions in the southern areas or the local accumulation of particulates in the stable ABL. In the nocturnal $PM_{2.5}$ enhancement events of non-T-NPES conditions in Changzhou, higher wind speeds in the ABL and predominantly from the northern and southwestern, which indicated the nocturnal $PM_{2.5}$ enhancement might result from horizontal transport from the NCP (Huang et al., 2020) or caused by other reasons. For example, from the perspective of chemical formation, the nocturnal atmospheric oxidation may elevate the nighttime aerosol concentration (Wang et al., 2023; Yan et al., 2023). In addition, we found the T-NPES event does not always cause a nocturnal $PM_{2.5}$ increase, in a few cases, the strong north wind following the cold front play a role in removing the aerosol. In summary, the T-NPES just represents one vertical transport mechanism that can collectively contribute to the enhancement of nocturnal $PM_{2.5}$ with other physical and chemical processes (Zhao et al., 2023). Further understanding of the coupling effect of transportation as well as the chemical formation to the nocturnal $PM_{2.5}$ enhancement is thus highly needed. Based on these mentioned above, we suggested that the T-NPES events were a common phenomenon in winter in plain areas such as the NCP and the YRD. A conceptual model was thus developed and shown in Figure 10, there was the transportation of aerosol by the horizontal winds in the high altitude and the updrafts dominated before night, which was conducive to the formation and suspension of the aerosol layer. Then, with the southeasterly movement of the high-pressure system and the passage of the cold front at about the time of midnight, the wind direction began to turn north/northwest, causing the aerosol to dilute. Finally, the downdrafts dominated in the ABL and the LLJ might enhance the turbulence. Under the influence of subsidence behind the cold front and turbulence, the depth of the aerosol layer suspended in the high altitude began to decrease and the pollutants gradually transported and diffused downwards into the lower layer of the ABL, enhancing the concentration of surface $PM_{2.5}$.

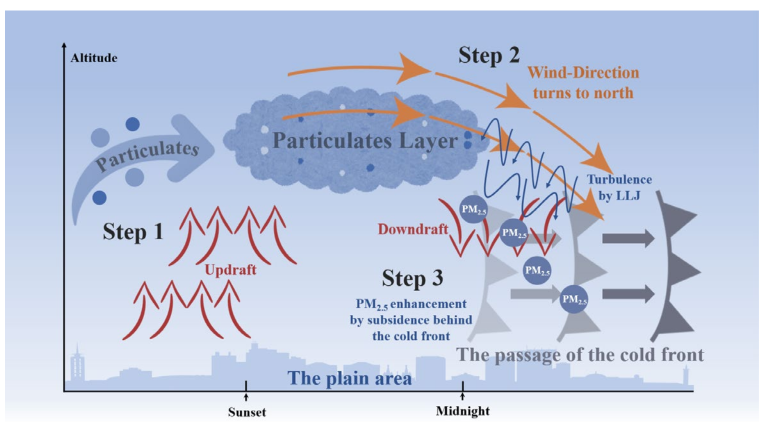

Figure 10. Conceptual scheme of the T-NPES events

3.4 No T-NPES event occurred in Basin areas

We further checked the fix-point measurement in Xi’an and Chengdu, two cities with typical basin topography. The results indicated that there were essentially no T-NPES events in either city, suggesting the concept did not work. Figure 11(a) indicated that the concentration of surface $PM_{2.5}$ had no enhancement during the night from 23:00 on 31 December to 4:00 on 1 January, and from 22:00 on 1 January to 3:00 on 2 January in Xi’an. $PM_{2.5}$ remained at a high concentration, while the extinction coefficient did not show the subsidence process, suggesting that the T-NPES events were not common here.

Taking the night of 31 December as an example, from 18:00 on 31 December to 4:00 on 1 January, the concentration of surface $PM_{2.5}$ increased before 23:00. Then it stabilized at high values, while the extinction coefficient remained at a high level with about 1.0-1.2 km^{-1} near 500 m. As shown in Figure 11(d), from 18:00, 31 December to 6:00, 1 January, a light wind layer appeared below 1,000 m, with ~1 m/s. Such a static and stable condition was conducive to the accumulation of locally generated particulate matter near the ground, causing the concentration of $PM_{2.5}$ to enhance between 18:00 and 23:00 on 31 December and the formation and maintenance of the aerosol layer at about 500 m. Noteworthy, the wind direction at the low layer was southeaster, while it was the opposite northwester at about 1,000 m, which was the typical characteristic of mountain-valley breeze circulation. The dominance of downdrafts below 500 m suggested that Xi'an was in the upper area of the nocturnal mountain-valley breeze circulation. The mountain-valley breeze circulation could only be observed when the background WS was relatively weak, which further indicated a stable structure of the ABL. The example on 1 January was similar to the above one, with the extinction coefficient reaching 2 km^{-1} and the depolarization ratio decreasing after 21:00 due to the hygroscopic growth of aerosol by the rise in relative humidity.

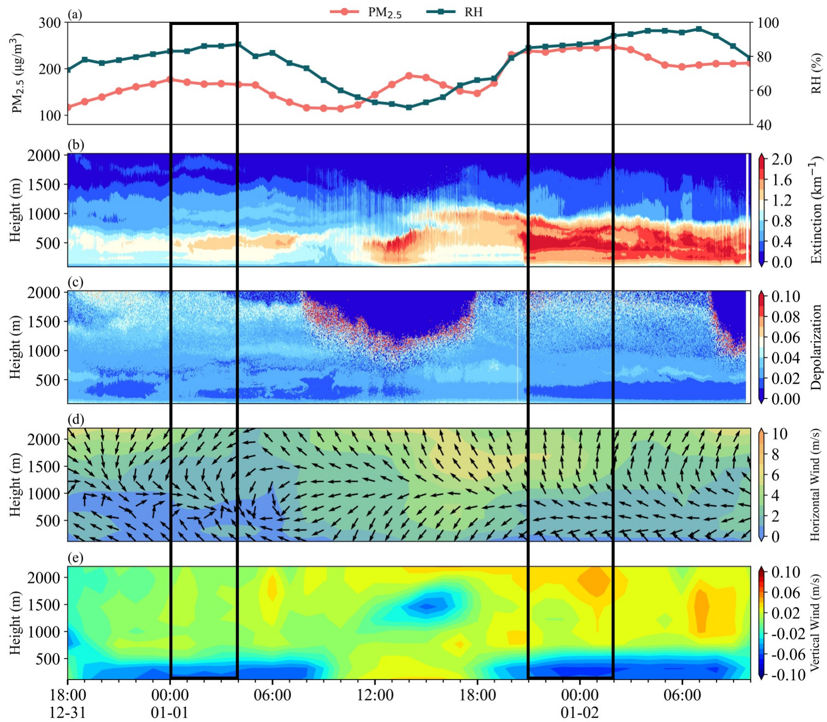

Figure 11. (a) Surface $PM_{2.5}$ concentration and relative humidity, (b) Extinction coefficient, (c) Depolarization ratio, (d) Horizontal wind, and (e) Vertical wind, during the observation in Xi'an from 18:00, 31 December to 10:00, 2 January. The two black boxes were the period to be studied.

Due to the topography of the basin in Xi'an, the mountain-valley breeze circulation, or the horizontal winds with lower WS always dominated the ABL, which was not conducive to the transport and dispersion of particulate matter. The stable structure of the ABL resulted in the particulate matter accumulating in the low layer, which was the main feature of the nocturnal particulate matter distribution in Xi'an.

Figure 12 showed that the concentration of surface $PM_{2.5}$ also had no significant enhancement but remained a high value over nighttime in Chengdu. The distribution of the extinction coefficient in the two black boxes presented a double-layer structure, one layer near 250 m and another layer suspended at about 500 m. Meanwhile, the wind field exhibited typical mountain-valley breeze circulation, as shown in the two black boxes in Figure 12(d), which presented westerly wind near 250 m and southeasterly wind above 500 m. The variation in wind direction due to the mountain-valley breeze circulation at different layers might be responsible for the double layer of particulate matter. Figure S10 illustrates the backward trajectories when the double-layer appeared. The layer of particulate matter at about 100 m might have originated from the southwest area of Chengdu, whereas the layer of particulate matter at 500 m and 1,000 m might have originated from the northeast area of Chengdu. The different sources of particulate matter were consistent with the mountain-valley breeze circulation in Chengdu, further demonstrating the dominance of the mountain-valley breeze in the static and stable ABL at night.

The orange box in Figure 12 indicated that the distribution of particulate matter in the ABL of Chengdu under the dominance of northeasterly winds with high WS. Both the extinction coefficient and the depolarization ratio showed a stratified structure, with the extinction coefficient initially higher below 750 m and lower above 750 m, whereas the depolarization ratio exhibited the opposite trend. The main cause of this phenomenon was that the different sources of particulate matter in the two layers. Under the influence of the dominant updrafts, local emissions with a high depolarization ratio were transported upwards, while the lower layer was occupied by particulate matter with a lower depolarization ratio transported by the northeasterly wind. As the continuous transport of the northeasterly wind, the entire ABL was occupied by transported particulate matter with a high extinction coefficient and a low depolarization ratio.

Due to the short time during the fixed-point observation period, it is difficult to make a universal conclusion that no T-NEPS occurs in basin regions. Therefore, we further checked the surface and model simulation data of the two basin cities for three months in winter 2018. We found that, unlike the plain area, the T-NEPS events were rarely observed in the basin regions. It confirmed that the conceptual model was indeed not applicable in the basin area. This was mainly attributed to the fact that the movement of the weather system was blocked by the mountains surrounding the basin. Therefore, the movement of the high-pressure system and the passage of the cold front had a weak impact on the basin region. Without the downdrafts and the shift in wind direction associated with the movement of the high-pressure system and the passage of the cold front, the structure of the ABL between Xi'an and Chengdu was relatively stable, making it difficult for particulate matter to be transported and diffused, and thus accumulate in the ABL at night. During the three months, we found that the wind field in Xi'an was dominated by light winds, while in Chengdu there were two states: one was dominated by light winds and the other by strong northeasterly winds. Fortunately, our fixed-point observations had captured these typical processes indeed. In addition, considering the wind fields in basin cities were mainly dominated by light winds, which was the main characteristic of basin area (Bei et al., 2016; Shu et al., 2021) and was similar to the wind fields below 1,500 m in Taiyuan and Linfen of the Type 4. Therefore, we suggested that the Loess Plateau cities might serve as a crucial transitional zone between the plains and the basin as introduced in Section 3.3. In summary, the conceptual model of T-NPES events was applicable to the plain areas which were more influenced by the movement of the weather system in winter, such as the NCP and YRD, but not to the basin areas.

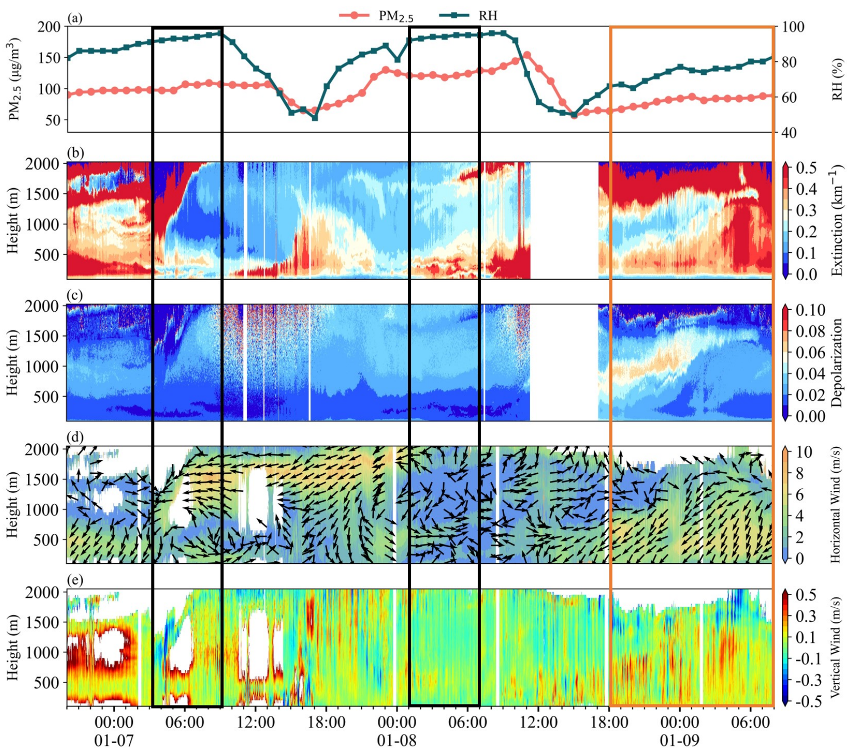

Figure 12. (a) Surface $PM_{2.5}$ concentration and relative humidity, (b) Extinction coefficient, (c) Depolarization ratio, (d) Horizontal wind, and (e) Vertical wind, during the observation in Chengdu from 20:00, 7 January to 8:00, 10 January. The two black boxes were the period of the double-layer structure, the orange box was the period to be studied.

4 Conclusions and outlook

In this study, we reveal that the T-NPES is a relatively common and important pathway that causes $PM_{2.5}$ pollution in the surface layer in plain areas in winter China. The fixed-point observations in Changzhou and Wangdu demonstrated that the T-NPES was associated with the subsidence of particulate matter in the upper layer due to the movement of high pressure and the passage of the cold front. Model simulations further confirmed the ubiquity of T-NPES events in plain areas, despite these event types varied case by case. However, the observations in Xi'an and Chengdu indicated that the event was less occurred in the basin areas, as the impact of the weather system was weakened by the obstruction of mountains surrounding the basin. In future studies, more multi-lidar measurements should be conducted in other cities in the plains and basin areas to look insight to the detailed mechanism of T-NPES events. In addition, more works are urgently needed to uncover the vertical profiles of chemical components of the particulate matter, since it may also be affected by the coupling of physical and chemical processes.

Code/Data availability. The datasets used in this study are available at: https://doi.org/10.5281/zenodo.8368944 (Wang et al., 2023).

Author contributions. H.C.W. and S.J.F designed the study. Y.M.W. and H.C.W. analyzed the data, H.L.W. and X.L. provided the GEOS-Chem model simulation results, and Y.M.W. and H.C.W. wrote the paper with input from all coauthors.

Competing interests. The authors declare that they have no conflicts of interest.

Acknowledgments. The authors gratefully acknowledge the NOAA Air Resources Laboratory (ARL) for the provision of the HYSPLIT transport and dispersion model used in this study.

Financial support. This research has been supported by the Guangdong Major Project of Basic and Applied Basic Research (grant no. 2020B0301030004), the National Research Program for Key Issue in Air Pollution Control (grant no. 2023YFC3709201, 2023YFC3706103, 2023YFC3710900), and the National Natural Science Foundation of China (grant no. 42175111), the Fundamental Research Funds for the Central Universities, Sun Yat-sen University (23lgbj002).

References

An, Z.S., Huang, R.J., Zhang, R.Y., Tie, X.X., Li, G.H., Cao, J.J., Zhou, W.J., Shi, Z.G., Han, Y.M., Gu, Z.L., Ji, Y.M.: Severe haze in northern China: A synergy of anthropogenic emissions and atmospheric processes. P. Natl. Acad. Sci. USA. 116, 8657-8666. http://doi.org/10.1073/pnas.1900125116, 2019

Bei, N.F., Xiao, B., Meng, N., Feng, T.: Critical role of meteorological conditions in a persistent haze episode in the Guanzhong basin, China. Sci. Total Environ., 550, 273-284. http://doi.org/10.1016/j.scitotenv.2015.12.159, 2016

Bey, I., Jacob, D.J., Yantosca, R.M., Logan, J.A., Field, B.D., Fiore, A.M., Li, Q.B., Liu, H.G.Y., Mickley, L.J., Schultz, M.G.: Global modeling of tropospheric chemistry with assimilated meteorology: Model description and evaluation. J. Geophys. Res.: Atmos., 106, 23073-23095. http://doi.org/10.1029/2001JD000807, 2001

Bian, H.S., Prather, M.J.: Fast-J2: Accurate simulation of stratospheric photolysis in global chemical models. J. Atmos. Chem., 41, 281-296. http://doi.org/10.1023/A:1014980619462, 2002

Cai, W.J., Li, K., Liao, H., Wang, H.J., Wu, L.X.: Weather conditions conducive to Beijing severe haze more frequent under climate change. Nat. Clim. Change. 7, 257-+. http://doi.org/10.1038/NCLIMATE3249, 2017

Callahan, C.W., Schnell, J.L., Horton, D.E.: Multi-Index Attribution of Extreme Winter Air Quality in Beijing, China. J. Geophys. Res.: Atmos., 124, 4567-4583. http://doi.org/10.1029/2018JD029738, 2019

Carlson, M.A., Stull, R.B.: Subsidence in the nocturnal boundary layer. J. Clim. Appl. Meteorol., 25, 1088-1099. http://doi.org/10.1175/1520-0450(1986)025<1088:sitnbl>2.0.co;2, 1986

Chen, X.R., Wang, H.C., Lu, K.D., Li, C.M., Zhai, T.Y., Tan, Z.F., Ma, X.F., Yang, X.P., Liu, Y.H., Chen, S.Y., Dong, H.B., Li, X., Wu, Z.J., Hu, M., Zeng, L.M., Zhang, Y.H.: Field Determination of Nitrate Formation Pathway in Winter Beijing. Environ. Sci. Technol., 54, 9243-9253. http://doi.org/10.1021/acs.est.0c00972, 2020

De Marco, A., Proietti, C., Anav, A., Ciancarella, L., D'Elia, I., Fares, S., Fornasier, M.F., Fusaro, L., Gualtieri, M., Manes, F., Marchetto, A., Mircea, M., Paoletti, E., Piersanti, A., Rogora, M., Salvati, L., Salvatori, E., Screpanti, A., Vialetto, G., Vitale, M., Leonardi, C.: Impacts of air pollution on human and ecosystem health, and implications for the National Emission Ceilings Directive: Insights from Italy. Environ. Int., 125, 320-333. http://doi.org/10.1016/j.envint.2019.01.064, 2019

Ding, A.J., Fu, C.B., Yang, X.Q., Sun, J.N., Petaja, T., Kerminen, V.M., Wang, T., Xie, Y., Herrmann, E., Zheng, L.F., Nie, W., Liu, Q., Wei, X.L., Kulmala, M.: Intense atmospheric pollution modifies weather: a case of mixed biomass burning with fossil fuel combustion pollution in eastern China. Atmos. Chem. Phys., 13, 10545-10554. http://doi.org/10.5194/acp-13-10545-2013, 2013

Ding, A.J., Huang, X., Nie, W., Chi, X.G., Xu, Z., Zheng, L.F., Xu, Z.N., Xie, Y.N., Qi, X.M., Shen, Y.C., Sun, P., Wang, J.P., Wang, L., Sun, J.N., Yang, X.Q., Qin, W., Zhang, X.Z., Cheng, W., Liu, W.J., Pan, L.B., Fu, C.B.: Significant reduction of $PM_{2.5}$ in eastern China due to regional-scale emission control: evidence from SORPES in 2011-2018. Atmos. Chem. Phys., 19, 11791-11801. http://doi.org/10.5194/acp-19-11791-2019, 2019

Dong, Z.P., Li, Z.Q., Yu, X., Cribb, M., Li, X.M., Dai, J.: Opposite long-term trends in aerosols between low and high altitudes: a testimony to the aerosol-PBL feedback. Atmos. Chem. Phys., 17, 7997-8009. http://doi.org/10.5194/acp-17-7997-2017, 2017

Dubey, R., Patra, A.K., Joshi, J., Blankenberg, D., Nazneen. Evaluation of vertical and horizontal distribution of particulate matter near an urban roadway using an unmanned aerial vehicle. Sci. Total Environ., 836. http://doi.org/10.1016/j.scitotenv.2022.155600, 2022

Fast, J.D., Bell, D.M., Kulkarni, G., Liu, J.M., Mei, F., Saliba, G., Shilling, J.E., Suski, K., Tomlinson, J., Wang, J., Zaveri, R., Zelenyuk, A.: Using aircraft measurements to characterize subgrid-scale variability of aerosol properties near the Atmospheric Radiation Measurement Southern Great Plains site. Atmos. Chem. Phys., 22, 11217-11238. http://doi.org/10.5194/acp-22-11217-2022, 2022

Gao, M., Carmichael, G.R., Wang, Y., Saide, P.E., Yu, M., Xin, J., Liu, Z., Wang, Z.: Modeling study of the 2010 regional haze event in the North China Plain. Atmos. Chem. Phys., 16, 1673-1691. http://doi.org/10.5194/acp-16-1673-2016, 2016

Gao, M., Liu, Z.R., Zheng, B., Ji, D.S., Sherman, P., Song, S.J., Xin, J.Y., Liu, C., Wang, Y.S., Zhang, Q., Xing, J., Jiang, J.K., Wang, Z.F., Carmichael, G.R., McElroy, M.B.: China's emission control strategies have suppressed unfavorable influences of climate on wintertime PM2.5 concentrations in Beijing since 2002. Atmos. Chem. Phys., 20, 1497-1505. http://doi.org/10.5194/acp-20-1497-2020, 2020

Gao, M., Saide, P.E., Xin, J.Y., Wang, Y.S., Liu, Z.R., Wang, Y.X., Wang, Z.F., Pagowski, M., Guttikunda, S.K., Carmichael, G.R.: Estimates of Health Impacts and Radiative Forcing in Winter Haze in Eastern China through Constraints of Surface $PM_{2.5}$ Predictions. Environ. Sci. Technol., 51, 2178-2185. http://doi.org/10.1021/acs.est.6b03745, 2017

Gelaro, R., McCarty, W., Suarez, M.J., Todling, R., Molod, A., Takacs, L., Randles, C.A., Darmenov, A., Bosilovich, M.G., Reichle, R., Wargan, K., Coy, L., Cullather, R., Draper, C., Akella, S., Buchard, V., Conaty, A., da Silva, A.M., Gu, W., Kim, G.K., Koster, R., Lucchesi, R., Merkova, D., Nielsen, J.E., Partyka, G., Pawson, S., Putman, W., Rienecker, M., Schubert, S.D., Sienkiewicz, M., Zhao, B.: The Modern-Era Retrospective Analysis for Research and Applications, Version 2 (MERRA-2). J. Clim., 30, 5419-5454. http://doi.org/10.1175/JCLI-D-16-0758.1, 2017

Geng, G.N., Xiao, Q.Y., Liu, S.G., Liu, X.D., Cheng, J., Zheng, Y.X., Xue, T., Tong, D., Zheng, B., Peng, Y.R., Huang, X.M., He, K.B., Zhang, Q.: Tracking Air Pollution in China: Near Real-Time $PM_{2.5}$ Retrievals from Multisource Data Fusion. Environ. Sci. Technol., 55, 12106-12115. http://doi.org/10.1021/acs.est.1c01863, 2021a

Geng, G.N., Zheng, Y.X., Zhang, Q., Xue, T., Zhao, H.Y., Tong, D., Zheng, B., Li, M., Liu, F., Hong, C.P., He, K.B., Davis, S.J.: Drivers of $PM_{2.5}$ air pollution deaths in China 2002-2017. Nat. Geosci., 14, 645-+. http://doi.org/10.1038/s41561-021-00792-3, 2021b

Gramsch, E., Caceres, D., Oyola, P., Reyes, E., Vasquez, Y., Rubio, M.A., Sanchez, G.: Influence of surface and subsidence thermal inversion on $PM_{2.5}$ and black carbon concentration. Atmos. Environ., 98, 290-298. http://doi.org/10.1016/j.atmosenv.2014.08.066, 2014

Guo, S., Hu, M., Zamora, M.L., Peng, J.F., Shang, D.J., Zheng, J., Du, Z.F., Wu, Z., Shao, M., Zeng, L.M., Molina, M.J., Zhang, R.Y.: Elucidating severe urban haze formation in China. P. Natl. Acad. Sci. USA. 111, 17373-17378. http://doi.org/10.1073/pnas.1419604111, 2014

Hao, X., Li, J.D., Wang, H.J., Liao, H., Yin, Z.C., Hu, J.L., Wei, Y., Dang, R.J.: Long-term health impact of PM2.5 under whole-year COVID-19 lockdown. Environ. Pollut., 290. http://doi.org/10.1016/j.envpol.2021.118118, 2021

He, C., Lu, X., Wang, H.L., Wang, H.C., Li, Y., He, G.W., He, Y.P., Wang, Y.R., Zhang, Y.L., Liu, Y.M., Fan, Q., Fan, S.J.: The unexpected high frequency of nocturnal surface ozone enhancement events over China: characteristics and mechanisms. Atmos. Chem. Phys., 22, 15243-15261. http://doi.org/10.5194/acp-22-15243-2022, 2022

He, Y.P., Xu, X.Q., Gu, Z.L., Chen, X.H., Li, Y.M., Fan, S.J.: Vertical distribution characteristics of aerosol particles over the Guanzhong Plain. Atmos. Environ., 255. http://doi.org/10.1016/j.atmosenv.2021.118444, 2021

Hu, X.-M., Klein, P.M., Xue, M., Zhang, F., Doughty, D.C., Forkel, R., Joseph, E., Fuentes, J.D.: Impact of the vertical mixing induced by low-level jets on boundary layer ozone concentration. Atmos. Environ., 70, 123-130. http://doi.org/10.1016/j.atmosenv.2012.12.046, 2013

Huang, R.J., Zhang, Y.L., Bozzetti, C., Ho, K.F., Cao, J.J., Han, Y.M., Daellenbach, K.R., Slowik, J.G., Platt, S.M., Canonaco, F., Zotter, P., Wolf, R., Pieber, S.M., Bruns, E.A., Crippa, M., Ciarelli, G., Piazzalunga, A., Schwikowski, M., Abbaszade, G., Schnelle-Kreis, J., Zimmermann, R., An, Z.S., Szidat, S., Baltensperger, U., El Haddad, I., Prevot, A.S.H.: High secondary aerosol contribution to particulate pollution during haze events in China. Nature. 514, 218-222. http://doi.org/10.1038/nature13774, 2014

Huang, X., Ding, A.J., Wang, Z.L., Ding, K., Gao, J., Chai, F.H., Fu, C.B.: Amplified transboundary transport of haze by aerosol-boundary layer interaction in China. Nat. Geosci., 13, 428-+. http://doi.org/10.1038/s41561-020-0583-4, 2020

Huang, X., Wang, Z.L., Ding, A.J.: Impact of Aerosol-PBL Interaction on Haze Pollution: Multiyear Observational Evidences in North China. Geophys. Res. Lett., 45, 8596-8603. http://doi.org/10.1029/2018GL079239, 2018

Kang, H.Q., Zhu, B., Gao, J.H., He, Y., Wang, H.L., Su, J.F., Pan, C., Zhu, T., Yu, B.: Potential impacts of cold frontal passage on air quality over the Yangtze River Delta, China. Atmos. Chem. Phys., 19, 3673-3685. http://doi.org/10.5194/acp-19-3673-2019, 2019

Kang, H.Q., Zhu, B., Liu, X.H., Shi, S.S., Hou, X.W., Lu, W., Yan, S.Q., Pan, C., Chen, Y.: Three-Dimensional Distribution of $PM_{2.5}$ over the Yangtze River Delta as Cold Fronts Moving Through. J. Geophys. Res.: Atmos., 126. http://doi.org/10.1029/2020JD034035, 2021

Kraus, H., Malcher, J., Schaller, E.: A nocturnal low level jet during PUKK. Bound.-Layer Meteorol. (Netherlands). 31, 187-195. http://doi.org/10.1007/bf00121177, 1985

Largeron, Y., Staquet, C.: Persistent inversion dynamics and wintertime PM_{10} air pollution in Alpine valleys. Atmos. Environ., 135, 92-108. http://doi.org/10.1016/j.atmosenv.2016.03.045, 2016

Li, H.Y., Cheng, J., Zhang, Q., Zheng, B., Zhang, Y.X., Zheng, G.J., He, K.B.: Rapid transition in winter aerosol composition in Beijing from 2014 to 2017: response to clean air actions. Atmos. Chem. Phys., 19, 11485-11499. http://doi.org/10.5194/acp-19-11485-2019, 2019a

Li, L., Lu, C., Chan, P.W., Lan, Z.J., Zhang, W.H., Yang, H.L., Wang, H.C.: Impact of the COVID-19 on the vertical distributions of major pollutants from a tower in the Pearl River Delta. Atmos. Environ., 276. http://doi.org/10.1016/j.atmosenv.2022.119068, 2022

Li, Z.Q., Guo, J.P., Ding, A.J., Liao, H., Liu, J.J., Sun, Y.L., Wang, T.J., Xue, H.W., Zhang, H.S., Zhu, B.: Aerosol and boundary-layer interactions and impact on air quality. Natl. Sci. Rev., 4, 810-833. http://doi.org/10.1093/nsr/nwx117, 2017

Li, Z.Q., Wang, Y., Guo, J.P., Zhao, C.F., Cribb, M., Dong, X.Q., Fan, J.W., Gong, D.Y., Huang, J.P., Jiang, M.J., Jiang, Y.Q., Lee, S.S., Li, H., Li, J.M., Liu, J.J., Qian, Y., Rosenfeld, D., Shan, S.Y., Sun, Y.L., Wang, H.J., Xin, J.Y., Yan, X., Yang, X., Yang, X.Q., Zhang, F., Zheng, Y.T.: East Asian Study of Tropospheric Aerosols and their Impact on Regional Clouds, Precipitation, and Climate (EAST-AIR(CPC)). J. Geophys. Res.: Atmos., 124, 13026-13054. http://doi.org/10.1029/2019JD030758, 2019b

Lin, J.T., McElroy, M.B.: Impacts of boundary layer mixing on pollutant vertical profiles in the lower troposphere: Implications to satellite remote sensing. Atmos. Environ., 44, 1726-1739. http://doi.org/10.1016/j.atmosenv.2010.02.009, 2010

Lu, K.D., Fuchs, H., Hofzumahaus, A., Tan, Z.F., Wang, H.C., Zhang, L., Schmitt, S.H., Rohrer, F., Bohn, B., Broch, S., Dong, H.B., Gkatzelis, G.I., Hohaus, T., Holland, F., Li, X., Liu, Y., Liu, Y.H., Ma, X.F., Novelli, A., Schlag, P., Shao, M., Wu, Y.S., Wu, Z.J., Zeng, L.M., Hu, M., Kiendler-Scharr, A., Wahner, A., Zhang, Y.H.: Fast Photochemistry in Wintertime Haze: Consequences for Pollution Mitigation Strategies. Environ. Sci. Technol., 53, 10676-10684. http://doi.org/10.1021/acs.est.9b02422, 2019

Lv, L., Xiang, Y., Zhang, T., Chai, W., Liu, W.: Comprehensive study of regional haze in the North China Plain with synergistic measurement from multiple mobile vehicle-based lidars and a lidar network. Sci. Total Environ., 721. http://doi.org/10.1016/j.scitotenv.2020.137773, 2020

Mao, J., Fan, S., Jacob, D.J., Travis, K.R.: Radical loss in the atmosphere from Cu-Fe redox coupling in aerosols. Atmos. Chem. Phys., 13, 509-519. http://doi.org/10.5194/acp-13-509-2013, 2013

Munoz-Sabater, J., Dutra, E., Agusti-Panareda, A., Albergel, C., Arduini, G., Balsamo, G., Boussetta, S., Choulga, M., Harrigan, S., Hersbach, H., Martens, B., Miralles, D.G., Piles, M., Rodriguez-Fernandez, N.J., Zsoter, E., Buontempo, C., Thepaut, J.N.: ERA5-Land: a state-of-the-art global reanalysis dataset for land applications. Earth Syst. Sci. Data. 13, 4349-4383. http://doi.org/10.5194/essd-13-4349-2021, 2021

O'Rourke, P.R., Smith, S.J., Mott, A., Ahsan, H., McDuffie, E.E., Crippa, M., Klimont, S., McDonald, B., Z., W., Nicholson, M.B., Feng, L., Hoesly, R.M., 2021. CEDS v-2021-04-21 Emission Data 1975-2019 (Version Apr-21-2021).

Park, R.J., Jacob, D.J., Field, B.D., Yantosca, R.M., Chin, M.: Natural and transboundary pollution influences on sulfate-nitrate-ammonium aerosols in the United States: Implications for policy. J. Geophys. Res.: Atmos., 109. http://doi.org/10.1029/2003JD004473, 2004

Parrella, J.P., Jacob, D.J., Liang, Q., Zhang, Y., Mickley, L.J., Miller, B., Evans, M.J., Yang, X., Pyle, J.A., Theys, N., Van Roozendael, M.: Tropospheric bromine chemistry: implications for present and pre-industrial ozone and mercury. Atmos. Chem. Phys., 12, 6723-6740. http://doi.org/10.5194/acp-12-6723-2012, 2012

Peng, J.F., Hu, M., Shang, D.J., Wu, Z.J., Du, Z.F., Tan, T.Y., Wang, Y.N., Zhang, F., Zhang, R.Y.: Explosive Secondary Aerosol Formation during Severe Haze in the North China Plain. Environ. Sci. Technol., 55, 2189-2207. http://doi.org/10.1021/acs.est.0c07204, 2021

Qin, Y., Li, J.Y., Gong, K.J., Wu, Z.J., Chen, M.D., Qin, M.M., Huang, L., Hu, J.L.: Double high pollution events in the Yangtze River Delta from 2015 to 2019: Characteristics, trends, and meteorological situations. Sci. Total Environ., 792. http://doi.org/10.1016/j.scitotenv.2021.148349, 2021

Ran, L., Deng, Z.Z., Wu, Y.F., Li, J.W., Bai, Z.X., Lu, Y., Zhuoga, D.Q., Bian, J.C.: Measurement report: Vertical profiling of particle size distributions over Lhasa, Tibet - tethered balloon-based in situ measurements and source apportionment. Atmos. Chem. Phys., 22, 6217-6229. http://doi.org/10.5194/acp-22-6217-2022, 2022

Shi, Y., Zeng, Q.C., Liu, L., Huo, J.T., Zhang, Z., Ding, W.C., Hu, F.: Observed Evidence That Subsidence Process Stabilizes the Boundary Layer and Increases the Ground Concentration of Secondary Pollutants. J. Geophys. Res.: Atmos., 127. http://doi.org/10.1029/2021JD035244, 2022

Shu, Z.Z., Liu, Y.B., Zhao, T.L., Xia, J.R., Wang, C.G., Cao, L., Wang, H.L., Zhang, L., Zheng, Y., Shen, L.J., Luo, L., Li, Y.Q.: Elevated 3D structures of $PM_{2.5}$ and impact of complex terrain-forcing circulations on heavy haze pollution over Sichuan Basin, China. Atmos. Chem. Phys., 21, 9253-9268. http://doi.org/10.5194/acp-21-9253-2021, 2021

Silver, B., Conibear, L., Reddington, C.L., Knote, C., Arnold, S.R., Spracklen, D.V.: Pollutant emission reductions deliver decreased $PM_{2.5}$-caused mortality across China during 2015-2017. Atmos. Chem. Phys., 20, 11683-11695. http://doi.org/10.5194/acp-20-11683-2020, 2020

Song, R.F., Wang, D.S., Li, X.B., Li, B., Peng, Z.R., He, H.D.: Characterizing vertical distribution patterns of $PM_{2.5}$ in low troposphere of Shanghai city, China: Implications from the perspective of unmanned aerial vehicle observations. Atmos. Environ., 265. http://doi.org/10.1016/j.atmosenv.2021.118724, 2021

Stein, A.F., Draxler, R.R., Rolph, G.D., Stunder, B.J.B., Cohen, M.D., Ngan, F.: NOAA'S HYSPLIT ATMOSPHERIC TRANSPORT AND DISPERSION MODELING SYSTEM. Bull. Am. Meteorol. Soc., 96, 2059-2077. http://doi.org/10.1175/BAMS-D-14-00110.1, 2015

Wang, D.F., Huo, J.T., Duan, Y.S., Zhang, K., Ding, A.J., Fu, Q.Y., Luo, J.H., Fei, D.N., Xiu, G.L., Huang, K.: Vertical distribution and transport of air pollutants during a regional haze event in eastern China: A tethered mega-balloon observation study. Atmos. Environ., 246. http://doi.org/10.1016/j.atmosenv.2020.118039, 2021

Wang, F., Li, Z.Q., Ren, X.R., Jiang, Q., He, H., Dickerson, R.R., Dong, X.B., Lv, F.: Vertical distributions of aerosol optical properties during the spring 2016 ARIAs airborne campaign in the North China Plain. Atmos. Chem. Phys., 18, 8995-9010. http://doi.org/10.5194/acp-18-8995-2018, 2018

Wang, H.C., Lu, K.D., Chen, X.R., Zhu, Q.D., Chen, Q., Guo, S., Jiang, M.Q., Li, X., Shang, D.J., Tan, Z.F., Wu, Y.S., Wu, Z.J., Zou, Q., Zheng, Y., Zeng, L.M., Zhu, T., Hu, M., Zhang, Y.H.: High N_2O_5 Concentrations Observed in Urban Beijing: Implications of a Large Nitrate Formation Pathway. Environ. Sci. Technol. Lett., 4, 416-420. http://doi.org/10.1021/acs.estlett.7b00341, 2017

Wang, H.C., Wang, H.L., Lu, X., Lu, K.D., Zhang, L., Tham, Y.J., Shi, Z.B., Aikin, K., Fan, S.J., Brown, S.S., Zhang, Y.H.: Increased night-time oxidation over China despite widespread decrease across the globe. Nat. Geosci., 16, 217-+. http://doi.org/10.1038/s41561-022-01122-x, 2023

Wang, Y.H., Logan, J.A., Jacob, D.J.: Global simulation of tropospheric O3-NOx-hydrocarbon chemistry. 2. Model evaluation and global ozone budget. J. Geophys. Res. (USA). 103, 10727-10755. http://doi.org/10.1029/98jd00157, 1998

Wesely, M.L.: Parameterization of surface resistances to gaseous dry deposition in regional-scale numerical models. Atmos. Environ., 23, 1293-1304. http://doi.org/10.1016/0004-6981(89)90153-4, 1989

WHO. WHO Global Air Quality Guidelines: Particulate Matter ($PM_{2.5}$ and PM_{10}), Ozone, Nitrogen Dioxide, Sulfur Dioxide and Carbon Monoxide, World Health Organization (WHO), Geneva, Switzerland., 2021

Xiao, Q.Y., Geng, G.N., Cheng, J., Liang, F.C., Li, R., Meng, X., Xue, T., Huang, X.M., Kan, H.D., Zhang, Q., He, K.B.: Evaluation of gap-filling approaches in satellite-based daily $PM_{2.5}$ prediction models. Atmos. Environ., 244. http://doi.org/10.1016/j.atmosenv.2020.117921, 2021a

Xiao, Q.Y., Zheng, Y.X., Geng, G.N., Chen, C.H., Huang, X.M., Che, H.Z., Zhang, X.Y., He, K.B., Zhang, Q.: Separating emission and meteorological contributions to long-term $PM_{2.5}$ trends over eastern China during 2000-2018. Atmos. Chem. Phys., 21, 9475-9496. http://doi.org/10.5194/acp-21-9475-2021, 2021b

Xu, X.Q., Xie, J.L., Li, Y.M., Miao, S.J., Fan, S.J.: Measurement report: Vehicle-based multi-lidar observational study of the effect of meteorological elements on the three-dimensional distribution of particles in the western Guangdong-Hong Kong-Macao Greater Bay Area. Atmos. Chem. Phys., 22, 139-153. http://doi.org/10.5194/acp-22-139-2022, 2022

Xu, Z.N., Huang, X., Nie, W., Shen, Y.C., Zheng, L.F., Xie, Y.N., Wang, T.Y., Ding, K., Liu, L.X., Zhou, D.R., Qi, X.M., Ding, A.J.: Impact of Biomass Burning and Vertical Mixing of Residual-Layer Aged Plumes on Ozone in the Yangtze River Delta, China: A Tethered-Balloon Measurement and Modeling Study of a Multiday Ozone Episode. J. Geophys. Res.: Atmos., 123, 11786-11803. http://doi.org/10.1029/2018JD028994, 2018

Yan, C., Tham, Y.J., Nie, W., Xia, M., Wang, H.C., Guo, Y.S., Ma, W., Zhan, J.L., Hua, C.J., Li, Y.Y., Deng, C.J., Li, Y.R., Zheng, F.X., Chen, X., Li, Q.Y., Zhang, G., Mahajan, A.S., Cuevas, C.A., Huang, D.D., Wang, Z., Sun, Y.L., Saiz-Lopez, A., Bianchi, F., Kerminen, V.M., Worsnop, D.R., Donahue, N.M., Jiang, J.K., Liu, Y.C., Ding, A.J., Kulmala, M.: Increasing contribution of nighttime nitrogen chemistry to wintertime haze formation in Beijing observed during COVID-19 lockdowns. Nat. Geosci., 16, 975-+. http://doi.org/10.1038/s41561-023-01285-1, 2023

Yin, C.Q., Xu, J.M., Gao, W., Pan, L., Gu, Y.X., Fu, Q.Y., Yang, F.: Characteristics of fine particle matter at the top of Shanghai Tower. Atmos. Chem. Phys., 23, 1329-1343. http://doi.org/10.5194/acp-23-1329-2023, 2023

Yue, X., Unger, N., Harper, K., Xia, X.G., Liao, H., Zhu, T., Xiao, J.F., Feng, Z.Z., Li, J.: Ozone and haze pollution weakens net primary productivity in China. Atmos. Chem. Phys., 17, 6073-6089. http://doi.org/10.5194/acp-17-6073-2017, 2017

Zhang, G., Gao, Y., Cai, W.J., Leung, L.R., Wang, S.X., Zhao, B., Wang, M.H., Shan, H.Y., Yao, X.H., Gao, H.W.: Seesaw haze pollution in North China modulated by the sub-seasonal variability of atmospheric circulation. Atmos. Chem. Phys., 19, 565-576. http://doi.org/10.5194/acp-19-565-2019, 2019a

Zhang, L.M., Gong, S.L., Padro, J., Barrie, L.: A size-segregated particle dry deposition scheme for an atmospheric aerosol module. Atmos. Environ., 35, 549-560. http://doi.org/10.1016/S1352-2310(00)00326-5, 2001

Zhang, Q., Zheng, Y.X., Tong, D., Shao, M., Wang, S.X., Zhang, Y.H., Xu, X.D., Wang, J.N., He, H., Liu, W.Q., Ding, Y.H., Lei, Y., Li, J.H., Wang, Z.F., Zhang, X.Y., Wang, Y.S., Cheng, J., Liu, Y., Shi, Q.R., Yan, L., Geng, G.N., Hong, C.P., Li, M., Liu, F., Zheng, B., Cao, J.J., Ding, A.J., Gao, J., Fu, Q.Y., Huo, J.T., Liu, B.X., Liu, Z.R., Yang, F.M., He, K.B., Hao, J.M.: Drivers of improved $PM_{2.5}$ air quality in China from 2013 to 2017. P. Natl. Acad. Sci. USA. 116, 24463-24469. http://doi.org/10.1073/pnas.1907956116, 2019b

Zhang, R.Y., Wang, G.H., Guo, S., Zarnora, M.L., Ying, Q., Lin, Y., Wang, W.G., Hu, M., Wang, Y.: Formation of Urban Fine Particulate Matter. Chem. Rev., 115, 3803-3855. http://doi.org/10.1021/acs.chemrev.5b00067, 2015

Zhang, W.H., Li, W.S., An, X.D., Zhao, Y.H., Sheng, L.F., Hai, S.F., Li, X.D., Wang, F., Zi, Z.F., Chu, M.: Numerical study of the amplification effects of cold-front passage on air pollution over the North China Plain. Sci. Total Environ., 833. http://doi.org/10.1016/j.scitotenv.2022.155231, 2022

Zhao, X.J., Zhao, P.S., Xu, J., Meng, W., Pu, W.W., Dong, F., He, D., Shi, Q.F.: Analysis of a winter regional haze event and its formation mechanism in the North China Plain. Atmos. Chem. Phys., 13, 5685-5696. http://doi.org/10.5194/acp-13-5685-2013, 2013

Zhao, X.X., Zhao, X.J., Liu, P.F., Chen, D., Zhang, C.L., Xue, C.Y., Liu, J.F., Xu, J., Mu, Y.J.: Transport Pathways of Nitrate Formed from Nocturnal N_2O_5 Hydrolysis Aloft to the Ground Level in Winter North China Plain. Environ. Sci. Technol. http://doi.org/10.1021/acs.est.3c00086, 2023

Zheng, B., Tong, D., Li, M., Liu, F., Hong, C.P., Geng, G.N., Li, H.Y., Li, X., Peng, L.Q., Qi, J., Yan, L., Zhang, Y.X., Zhao, H.Y., Zheng, Y.X., He, K.B., Zhang, Q.: Trends in China's anthropogenic emissions since 2010 as the consequence of clean air actions. Atmos. Chem. Phys., 18, 14095-14111. http://doi.org/10.5194/acp-18-14095-2018, 2018

Zhou, X., Huang, X., Sun, P., Chi, X., Ren, C., Lai, S., Wang, Z., Qi, X., Wang, J., Nie, W., Xu, Z., Huo, J., Fu, Q., Ding, A.: Fast Secondary Aerosol Formation in Residual Layer and Its Impact on Air Pollution Over Eastern China. J. Geophys. Res.: Atmos., 128, e2023JD038501. http://doi.org/https://doi.org/10.1029/2023JD038501, 2023